Characterization and formation of NV centers in 3C, 4H, and 6H SiC: An *ab initio* study

A. Csóré,[1] H. J. von Bardeleben,[2] J. L. Cantin,[2] and A. Gali[3,1,*]

[1]*Department of Atomic Physics, Budapest University of Technology and Economics, Budafoki út 8, H-1111 Budapest, Hungary*

[2]*Sorbonne Universités, UPMC Université Paris 06, Centre National de la Recherche Scientifique, UMR 7588, Institut des NanoSciences de Paris, 75005 Paris, France*

[3]*Wigner Research Centre for Physics, Hungarian Academy of Sciences, P.O. Box 49, Budapest H-1525, Hungary*

(Received 18 May 2017; revised manuscript received 18 July 2017; published 16 August 2017)

Fluorescent paramagnetic defects in solids have become attractive systems for quantum information processing in recent years. One of the leading contenders is the negatively charged nitrogen-vacancy (NV) defect in diamond with visible emission, but an alternative solution in a technologically mature host is an immediate quest for many applications in this field. It has been recently found that various polytypes of silicon carbide (SiC), that are standard semiconductors with wafer scale technology, can host a NV defect that could be an alternative qubit candidate with emission in the near infrared region. However, there is much less known about this defect than its counterpart in diamond. The inequivalent sites within a polytype and the polytype variations offer a family of NV defects. However, there is an insufficient knowledge on the magneto-optical properties of these configurations. Here we carry out density functional theory calculations, in order to characterize the numerous forms of NV defects in the most common polytypes of SiC including 3C, 4H, and 6H, and we also provide new experimental data in 4H SiC. Our calculations mediate the identification of individual NV qubits in SiC polytypes. In addition, we discuss the formation of NV defects in SiC, providing detailed ionization energies of NV defects in SiC, which reveals the critical optical excitation energies for ionizing these qubits in SiC. Our calculations unravel the challenges to produce NV defects in SiC with a desirable spin bath.

DOI: 10.1103/PhysRevB.96.085204

I. INTRODUCTION

In recent years spin carrying defects in solids have proved to be highly suitable for qubit [1,2] and nanoscale sensor applications [3]. So far the most investigated defect is the negatively charged nitrogen-vacancy defect (NV center) in diamond [4–6] for which the afore-mentioned applications have been achieved. The exceptional properties of the NV center in diamond are related to its optically polarizable spin triplet ($S = 1$) ground state ($^3A_2$), a spin dependent radiative recombination from the excited ^3E triplet state, and a parallel operating spin selective nonradiative decay via intermediate singlet states ($^1A_1$, ^1E). This mechanism results in the strong spin polarization of the $^3A_2$ ground state with a predominant population of the $m_s = 0$ state. In addition, the spin state of the $^3A_2$ state can be read out optically even at room temperature due to the long spin-coherence times [4,7] via the optically detected magnetic resonance (ODMR) effect.

Despite the unique properties of the NV center in diamond, the material properties of diamond are not optimal and are difficult to integrate into existing semiconductor device technology. In addition, the visible emission of the NV center in diamond is not favorable for quantum communication where the fiber optics provides the most efficient transmission at near infrared (NIR) wavelengths. Alternative qubits in technologically mature materials for various quantum technology applications are much sought after. One of the most favorable candidates is silicon carbide with hosting divacancy defects that consist of adjacent carbon and silicon vacancies in the SiC lattice [1,7–10]. This defect exhibits very similar properties to those of the NV center in diamond, including the optical coherent control of this $S = 1$ center [1], and a relatively high contrast optical readout at resonant excitation [10], but it emits in the NIR region (around 1100-nm wavelength) not far from the telecom wavelengths. NIR emission is also desirable for *in vivo* fluorescent biosensor applications where fabrication of nanocrystalline SiC hosting NIR color centers has already been suggested to this end [11,12].

Very recently, the equivalent of the NV center in diamond, the N_CV_{Si} centers have been identified in different (3C,4H,6H) polytypes of SiC [13–15]. In the negative charge state they are spin $S = 1$ centers with optical properties shifted to the NIR region (around 1200-nm wavelength) almost compatible with the transmission wavelength of optical fibers. However, some of their optical properties and excited-state configurations have not yet been fully resolved either in experiments [13,15] or in theory [1,15–17] and thus require further investigations. Since qubits are individual quantum objects, thorough characterization of the individual NV defects in SiC is required to optimize the conditions of qubit operations. To this end, we carried out density functional theory (DFT) calculations of nitrogen-vacancy defects in 3C, 4H, and 6H SiC. We provide detailed results concerning their electronic structure, magneto-optical parameters, ionization energies, and formation energies. We also discuss the possible formation processes of NV defects in SiC and briefly compare the formation and ionization energies of the NV center and divacancy defects in SiC.

In the following, we describe the computational methods in Sec. III. Our results are presented in detail in Sec. IV where we compare them to the experimental data if available. Here, we show new electron paramagnetic resonance (EPR) spectra for basal NV centers in 4H SiC. We discuss the photoionization and the formation of the NV center in SiC in Sec. V. Finally, we conclude our paper in Sec. VI.

*gali.adam@wigner.mta.hu

 ©2017 American Physical Society

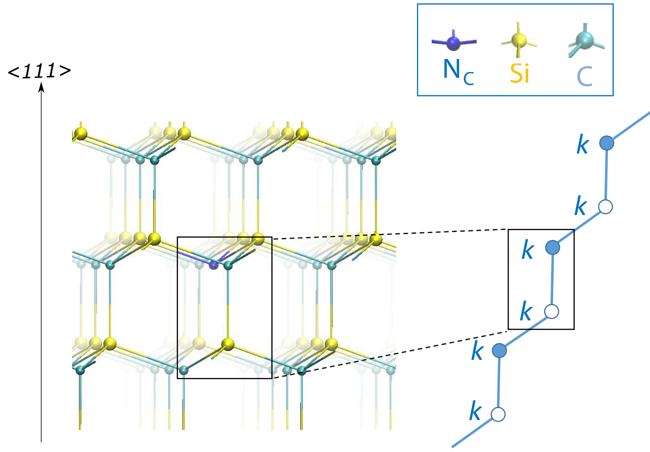

FIG. 1. Single configuration (kk) of N_CV_{Si} defect in 3C SiC.

II. DEFECT STRUCTURE

SiC exhibits various crystal structures, called polytypes, with 4H, 6H, and 3C the most advanced from a material point of view. We have therefore calculated the properties of the NV center in these technologically important polytypes. We found by *ab initio* calculations that formation energy of the N_CV_{Si} defect is lower by about 2 eV than that of the $N_{Si}V_C$ defect in each considered polytype in the neutral charged state, implying that nitrogen preferentially substitutes carbon (N_C) in the SiC lattice, adjacent to a neighbor Si vacancy (V_{Si}). We show the results on N_CV_{Si} in detail that we also call the NV center in this context.

Due to the special arrangement of the atoms in hexagonal polytypes, different varieties of the NV center exist, depending on the lattice site of the N atom and the adjacent Si vacancy. In short, the N_CV_{Si} defect forms one configuration in 3C (kk) (see Fig. 1), four configurations in 4H (hh, kk, hk, kh) (see Fig. 2), and six configurations in 6H (hh, k_1k_1, k_2k_2, hk_1, k_1k_2, k_2h) (see Fig. 3) polytypes, where h and $k_{\{1,2\}}$ label the hexagonal and (quasi)cubic lattice sites in each polytype, respectively.

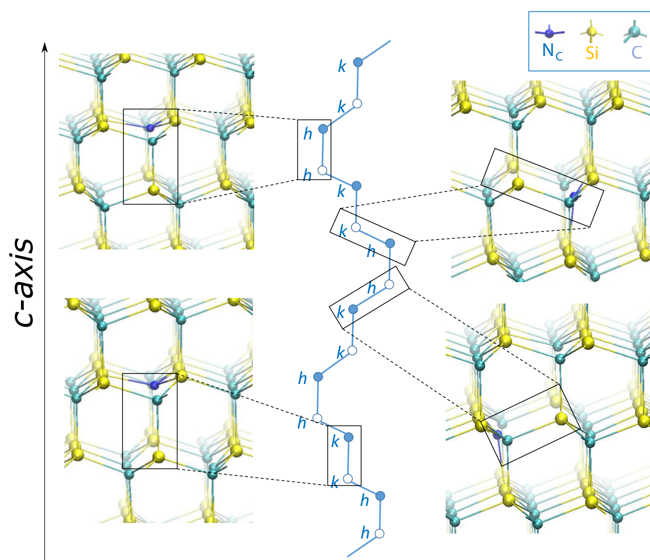

FIG. 2. Possible configurations of N_CV_{Si} defect in 4H SiC. The hh and kk configurations exhibiting C_{3v} symmetry are called *on-axis* configurations, since the axis of defects is parallel to the c axis, while kh and hk configurations are *off-axis* geometries with C_{1h} symmetry.

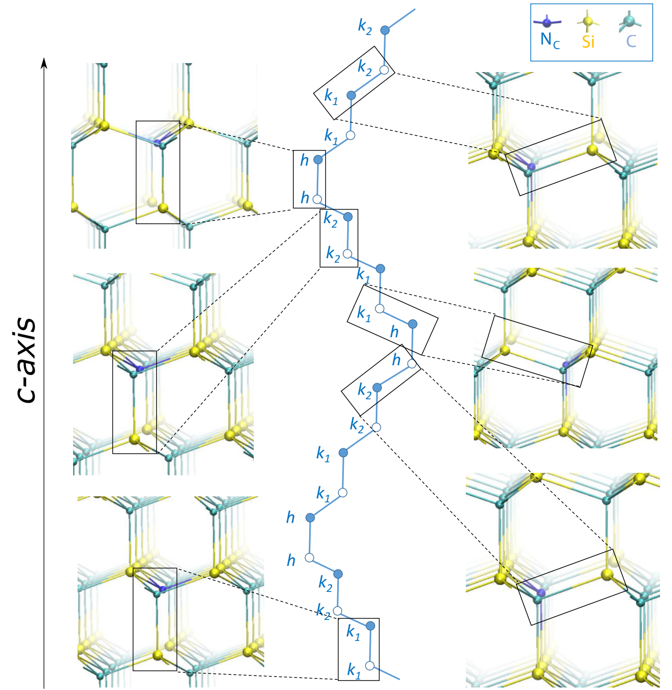

FIG. 3. Possible configurations of N_CV_{Si} defect structure in 6H SiC. Three on-axis (hh, k_1k_1, k_2k_2) and three off-axis or basal configurations (hk_1, k_1k_2, k_2h) can be formed.

III. METHODOLOGY

A. Computational approach

Our calculations were carried out by means of the HSE06 range-separated hybrid functional developed by Heyd, Scuseria, and Ernzerhof [18]. In order to characterize ground- and excited-state zero-field splitting (ZFS) arising from electron-spin–electron-spin–dipole-dipole interaction we calculated the D and E parameters employing the Perdew-Burke-Ernzerhof [19] functional as implemented by Ivády *et al.* [20]. In the excited state, on-axis defect configurations exhibit dynamic Jahn-Teller (JT) distortion due to an effective electron-phonon coupling, thus ZFS constants calculated under C_{1h} symmetry were averaged to show a dynamic C_{3v} symmetry. For basal configurations the natural symmetry is *per se* C_{1h} symmetry, nevertheless similar electron-phonon coupling can occur in the excited state as for the axial configurations. Therefore, we carried out a motional averaging procedure about the NV axis for the basal NV configurations. In the calculation of zero-phonon lines (ZPL) we used the lowest total energy in the excited state corresponding to the JT geometry.

For atomistic modeling of defect structures, we applied a 512-atom supercell for 3C, 576-atom supercell for 4H, and 432-atom supercell for 6H polytypes. For sampling the Brillouin zone we employed the Γ point only for 3C and 4H polytypes, while a Γ-centered $2 \times 2 \times 2$ Monkhorst-Pack k-point mesh was used for 6H SiC. In addition, to reach sufficient accuracy for ZPL values a $2 \times 2 \times 2$ k-point

mesh was employed in each case. Plane-wave expansion of Kohn-Sham wave functions with a cutoff of 420 eV was applied. Relaxed geometries were achieved by minimizing the total energy with respect to the normal coordinates of the lattice using the force threshold of 0.01 eV/Å. Core electrons were treated by projector-augmented wave [21] potentials as implemented in the VASP code [22]. In the case of charged defects Freysoldt correction [23] in total energy was applied. The hyperfine couplings were calculated by HSE06 DFT calculations taking into account the spin polarization of the core electrons [24].

B. Formation energies and charge transition levels

Concentration of point defects in thermal equilibrium can be predicted via the formation energies. In addition, determining the adiabatic charge transition levels, i.e., ionization energies, is also crucial to study the stability window of a given charge state of the defect that is applied as a qubit. We calculated the formation energies as [25,26]

$$E^q_{\mathrm{form}} = E^q_{\mathrm{tot}} - \frac{n_{\mathrm{Si}} + n_{\mathrm{C}}}{2}\mu_{\mathrm{SiC}} - \frac{\mu_{\mathrm{Si}} - \mu_{\mathrm{C}} - \delta\mu}{2}(n_{\mathrm{Si}} - n_{\mathrm{C}}) - n_{\mathrm{N}}\mu_{\mathrm{N}} + q(E_{\mathrm{f}} + E_{\mathrm{VBM}}) + \Delta V(q), \quad (1)$$

where E^q_{tot} is the total energy of the defective system; $\mu_{\mathrm{Si}},\mu_{\mathrm{C}},\mu_{\mathrm{N}}$ are the chemical potentials of the Si atom in bulk Si, the C atom in diamond, and the N atom, respectively; μ_{SiC} is the chemical potential of an Si-C unit in SiC crystal; n_{Si} and n_{C} are the number of Si and C atoms in the supercell, respectively; q is the charge state; E_{f} is the Fermi level; E_{VBM} represents the valence-band edge; and $\Delta V(q)$ stands for the Freysoldt charge correction term [23]. If $\delta\mu$ is chosen to be the heat of formation of SiC, $\mu_{\mathrm{SiC}} - (\mu_{\mathrm{Si}} + \mu_{\mathrm{C}})$, then this provides the formation energy of defects under stoichiometric conditions. In the actual VASP parameters and implementation we obtained $\mu_{\mathrm{SiC}} = -17.47$ eV, $\mu_{\mathrm{Si}} = -6.43$ eV, $\mu_{\mathrm{C}} = -10.55$ eV, and $\delta\mu = -0.49$ eV by HSE06. For determining μ_{N} the hexagonal β-Si_3N_4 was chosen as the most stable form of Si_3N_4 that can be considered as the solubility-limiting phase in SiC. We obtained $\mu_{\mathrm{N}} = -12.22$ eV upon these conditions. The adiabatic charge transition levels can be derived from Eq. (1) as follows:

$$E_{q+1/q} = E^q_{\mathrm{tot}} - E^{q+1}_{\mathrm{tot}} + \Delta V(q) - \Delta V(q+1). \quad (2)$$

Binding energy (E_{binding}) of defects A and B forming the complex AB can be defined as

$$E_{\mathrm{binding}}(E_{\mathrm{f}}) = E^{\mathrm{A}}_{\mathrm{form}}(E_{\mathrm{f}}) + E^{\mathrm{B}}_{\mathrm{form}}(E_{\mathrm{f}}) - E^{\mathrm{AB}}_{\mathrm{form}}(E_{\mathrm{f}}). \quad (3)$$

According to this definition $E_{\mathrm{binding}} > 0$ implies that the formation of the AB complex is favorable.

C. Calculation of defect concentrations

Defects may be introduced during growth of the crystal. High-quality silicon carbide is typically grown via the chemical vapor deposition process that may be considered as a quasiequilibrium process. The concentration of defects can be then estimated in thermal equilibrium at the growth temperatures. The concentration of a defect D^q with charge state q is the sum of the concentration of individual configurations D^q_i, i.e., symmetry inequivalent forms of D^q. This can be calculated by multiplying the number of possible defect sites per cm^3 ($N^{\mathrm{D}}_{\mathrm{sites}}$) by the statistical weight ω_{D^q} coming from the spin multiplicity and the Boltzmann factor

$$[\mathrm{D}^q(E_{\mathrm{f}})] = \sum_{\mathrm{i}} [\mathrm{D}^q_i(E_{\mathrm{f}})] = \frac{1}{Z} N^{\mathrm{D}}_{\mathrm{sites}}\omega_{D^q} \sum_{\mathrm{i}} \exp\left(-\frac{E^{\mathrm{D}^q_i}_{\mathrm{form}}(E_{\mathrm{f}})}{k_{\mathrm{B}}T}\right), \quad (4)$$

where

$$Z = 1 + \sum_{i,q} \omega_{D^q} \exp\left(-\frac{E^{\mathrm{D}^q_i}_{\mathrm{form}}(E_{\mathrm{f}})}{k_{\mathrm{B}}T}\right) \quad (5)$$

is the grand canonical partition function and the summation goes over all the individual configurations (i) and charge states (q) of defect D. In Eqs. (4) and (5) k_{B} is the Boltzmann constant and T is the temperature. For calculating $E^{\mathrm{D}^q_i}_{\mathrm{form}}(E_{\mathrm{f}})$ Fermi energy has to be determined [Eq. (1)], which can be performed via solving the neutrality equation, which reads as

$$N_c(T)\exp\left(-\frac{E_{\mathrm{CBM}} - E_{\mathrm{f}}}{k_{\mathrm{B}}T}\right) + \sum_{\substack{\mathrm{D} \\ q<0}} |q_{\mathrm{D}}|[\mathrm{D}^q(E_{\mathrm{f}})] = N_v(T)\exp\left(-\frac{E_{\mathrm{f}} - E_{\mathrm{VBM}}}{k_{\mathrm{B}}T}\right) + \sum_{\substack{\mathrm{D} \\ q>0}} |q_{\mathrm{D}}|[\mathrm{D}^q(E_{\mathrm{f}})], \quad (6)$$

where

$$N_c(T) = 2\left(\frac{2m^*_{\mathrm{e}}\pi k_{\mathrm{B}}T}{h^2}\right)^{3/2} \quad (7)$$

and

$$N_v(T) = 2\left(\frac{2m^*_{\mathrm{h}}\pi k_{\mathrm{B}}T}{h^2}\right)^{3/2} \quad (8)$$

are the effective densities of states of electrons in the conduction-band edge and holes in the valence-band edge, respectively, and E_{CBM} and E_{VBM} label the conduction- and valence-band edges, respectively. We applied the parameters of 4H SiC as we calculated the concentration of defects in this polytype. Accordingly, for the effective masses in Eqs. (7) and (8) we used $m^*_{\mathrm{h}} = 1.26m^0_{\mathrm{e}}$ and $m^*_{\mathrm{e}} = 0.39m^0_{\mathrm{e}}$, where m^0_{e} is the electron rest mass. We note that the shallow substitutional nitrogen donors in SiC will be explicitly treated in Eq. (4).

In order to obtain Fermi energy the series of equations [Eqs. (4) and (6)] has to be solved self-consistently. For the calculation, thermal equilibrium and stoichiometric ratio of C and Si atoms were assumed. We considered infinite bulk material, thus the effect of band bending near the surface and other kinetic effects were neglected. Bulk growth of SiC is usually carried out at temperatures between 1600 and 2000 °C [27,28]. Employing this technique different charge states of substitutional nitrogen ($\mathrm{N_C}$), vacancies ($\mathrm{V_C}$, $\mathrm{V_{Si}}$), divacancies ($\mathrm{V_CV_{Si}}$), carbon antisite vacancy pairs (CAV), and nitrogen-vacancy complexes [$(\mathrm{N_C})_k\mathrm{V_{Si}}$, $k = 1,2,3,4$] may be formed. For nitrogen-vacancy complexes we considered the case of $k = 1$ ($\mathrm{N_CV_{Si}}$) and the electrically inactive $k = 4$ [$(\mathrm{N_C})_4\mathrm{V_{Si}}$ defect] as the latter has an extremely low formation energy

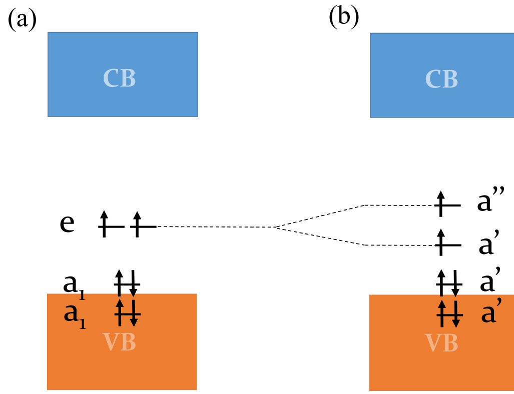

FIG. 4. Scheme of ground-state electronic structure of (a) on-axis and (b) off-axis NV center configurations exhibiting C_{3v} and C_{1h} symmetry, respectively.

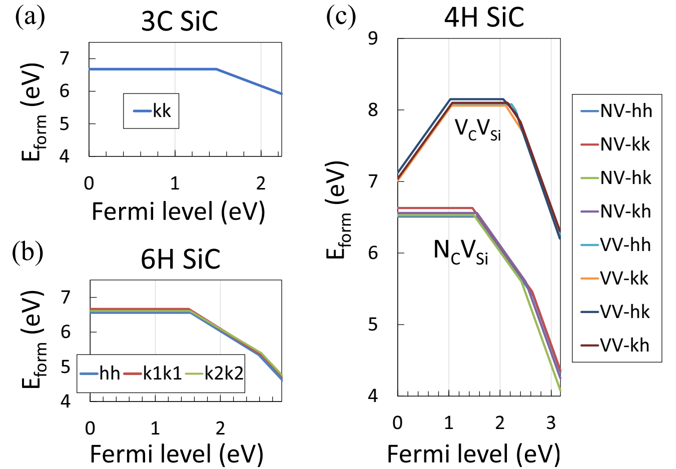

FIG. 5. Formation energies of the NV defects as a function of the position of the Fermi level in (a) 3C, (b) 6H, and (c) 4H polytypes. In 4H SiC we plot the formation energy of V_CV_{Si} divacancy.

[29]. In this spirit, we calculated the concentrations of the these defects at temperatures of 1600, 1700, 1800, 1900, and 2000 °C considering all relevant charge states. To this end, we calculated the formation energies of all the defects in all configurations including V_{Si}, V_C, and CAV [30–32].

IV. RESULTS

By using the HSE06 functional we could reproduce the experimental band gap within 0.1 eV for 3C, 4H, and 6H polytypes. This limits the accuracy of our method in the prediction of charge transition levels.

A. Electronic structure

Group theory analysis on the defect provides intriguing insights its electronic structure. Accordingly, we found that on-axis configurations of the NV center with C_{3v} symmetry introduce two a_1 levels and a degenerate e level. Off-axis configurations exhibit C_{1h} symmetry, and the degenerate e level splits to an a' and an a'' state while the a_1 states transform into a' states. Our calculations revealed that one of the a_1 levels falls in the valence band, whereas the other is lying in the fundamental band gap and they both are fully occupied. In the single negative charged state, the degenerate e level is introduced in the band gap occupied by two electrons with parallel spins providing the $S = 1$ triplet spin state. In summary, the one-electron structure of the ground state is $a_1(2)a_1(2)e(2)$ for on-axis and $a'(2)a'(2)a'(1)a''(1)$ for off-axis configurations in the singly negative charge state (see Fig. 4). Further application of group theory implies that $^3A_2$, ^1E, and $^1A_1$ multiplets can be formed by the $a_1(2)a_1(2)e(2)$ electron configurations for the on-axis defects. The ^3E bright triplet excited state is realized by $a_1(2)a_1(1)e(3)$ electron configuration, and an ^1E multiplet occurs too for on-axis defects. The ^3E excited state is a dynamic Jahn-Teller system. We calculated this excited state by ΔSCF method allowing C_{1h} symmetry distortion but the zero-field constant was calculated in the dynamic average of C_{3v} symmetry. For the off-axis configurations, the electronic configurations and states are similar to those of on-axis configurations, but the degenerate states are split due to the C_{1h} symmetry crystal field.

B. Formation energies and charge state stability of NV centers in SiC

We plot the formation energies of the NV defect in the considered polytypes of SiC in Fig. 5. We find that the neutral and negative charged states are stable as a function of the position of the Fermi level in all the polytypes, whereas the double negative charged state exists in hexagonal polytypes. The negatively charged NV defect, i.e., the NV center, can occur in moderately or highly n-type 3C SiC, whereas the NV center is stable in nondoped or moderately n-type doped hexagonal SiC. In highly n-type doped hexagonal SiC, the NV defect becomes double negatively charged. This result implies that different doping strategies should be applied to stabilize the single negative charge state of the NV defect in cubic and hexagonal polytypes.

We find that the formation energies of N_CV_{Si} defect configurations in 4H and 6H polytypes vary slightly, i.e., the values agree within ∼0.1 eV, whereas the maximum difference between the corresponding charge transition levels does not exceed ∼0.2 eV (see Table I). In Fig. 5(c) formation energies of V_CV_{Si} configurations in the 4H polytype are also showed for discussion.

C. Magneto-optical properties of NV centers in SiC

The NV centers in all three polytypes have the same electronic structure with a $^3A_2$ triplet ground state and

TABLE I. Charge transition levels of N_CV_{Si} defects referenced to the valence-band maximum (E_{VBM}).

Polytype	Conf.	$E_{0/-}$ (eV)	$E_{-/2-}$ (eV)
3C	kk	1.48	
4H	hh	1.54	2.65
	kk	1.46	2.63
	hk	1.49	2.42
	kh	1.55	2.50
6H	hh	1.54	2.59
	k_1k_1	1.51	2.64
	k_2k_2	1.53	2.62

TABLE II. Calculated hyperfine constants ($A_{ii}; i = x,y,z$) in the ground state of on-axis NV center configurations. Experimental data [15] available for the ^{14}N isotope (A^{iso}_{exp}) are also listed.

Polytype	Conf.	$1 \times {}^{14}$N A^{iso}_{exp}(MHz)	$1 \times {}^{14}$N A_{xx}, A_{yy}, A_{zz} (MHz)	$3 \times {}^{29}$Si + $6 \times {}^{29}$Si A_{xx}, A_{yy}, A_{zz} (MHz)	A_{xx}, A_{yy}, A_{zz} (MHz)	$3 \times {}^{13}$C A_{xx}, A_{yy}, A_{zz} (MHz)
3C	kk	1.26	−1.67, −1.67, −1.72	11.93, 11.91, 12.31	9.64, 8.47, 10.48	48.23, 47.49, 119.38
4H	hh	1.23	−1.57, −1.57, −1.64	11.80, 11.72, 12.14	9.95, 8.77, 10.79	45.49, 44.86, 116.78
	kk	1.12	−1.71, −1.69, −1.71	12.77, 12.39, 13.26	10.56, 9.60, 11.32	42.23, 41.48, 112.79
6H	hh	1.32	−1.61, −1.61, −1.80	11.95, 11.84, 12.30	9.81, 8.74, 10.69	42.40, 41.81, 113.84
	k_1k_1	1.21	−1.76, −1.75, −1.76	12.94, 12.63, 13.48	10.93, 10.17, 11.74	37.00, 36.33, 108.14
	k_2k_2	1.26	−1.73, −1.73, −1.76	12.05, 12.00, 12.48	10.51, 9.51, 11.39	42.44, 41.78, 114.36

an ^3E excited state. The paramagnetic ground state makes them suitable to EPR spectroscopy, which has been applied successfully for their assessment [13–15]. Our calculations show in accordance with the experimental results that each type of the NV center is characterized by specific ZFS parameters, hyperfine (HF) interactions, and optical properties as shown in Tables II–IV.

We first discuss the spin-density distributions. In the ground state, the major spin density is localized on the three neighbor C atoms of the Si vacancy (see Fig. 6), providing a strong HF interaction with the ^{13}C nuclear spins. The HF interactions with the ^{14}N neighbor and its adjacent three ^{29}Si nuclei are small (≈1 MHz). Nevertheless, due to the small EPR linewidth of 0.02 mT they are already resolved and represent the fingerprint of NV centers which distinguish them from other defects in SiC. The Si atoms near the nearest-neighbor C atoms have stronger HF constants of ≈10 MHz, also resolved in the EPR spectra. The small value of the ^{14}N HF constants is due to the only indirect HF interaction; the calculational accuracy for these values is smaller than for the HF with the ^{13}C and ^{29}Si neighbors with direct HF interaction and estimated to 10% according to our tests on related defects [24]. Nevertheless, the calculated values are in good agreement with the experimental findings, as shown in Table II.

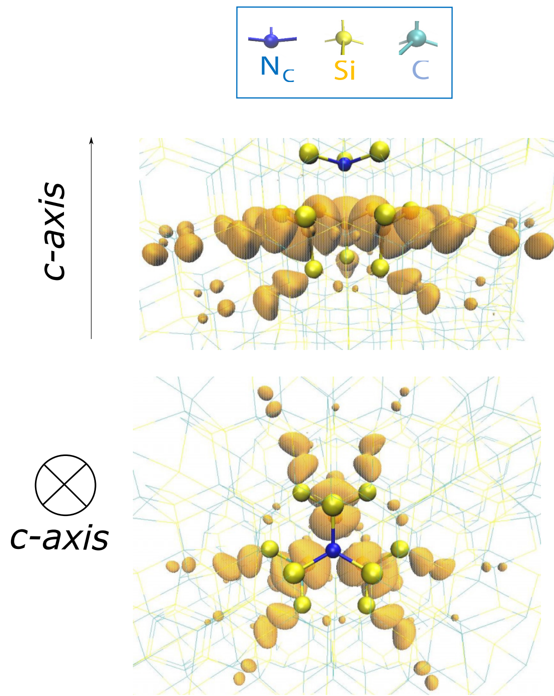

FIG. 6. Isosurface of the spin density localized on the three C atoms near the C vacancy in the triplet ground state of the NV center in SiC. The supercell structure is shown in perspective view where the lattice is depicted as a wire except for the atoms in the core of the defect that are represented by balls. The corresponding atom types are labeled.

We also determined the ZFS parameters (D, E) for NV centers by assuming electron-spin–electron-spin–dipolar interaction. We calculated these parameters in the $^3A_2$ ground state for all the considered polytypes (Tables III and IV). In the point-dipole-spin–point-dipole-spin approximation, the D varies as $D \sim \frac{1}{r^3}$ with r being the distance between the dipoles. In the ground state, the spin density is localized on the C atoms near the Si vacancy, so the distance between these C atoms gives the trend for the variation of the D constants (see Tables III and IV).

Here, we also report new EPR spectra of the basal NV centers in 4H SiC which have been measured in the temperature range from 4 to 300 K. To allow comparison with the calculated values, we show in Table III their parameters at T = 4 K. The NV centers in the 4H polytype were created as reported in Refs. [13–15] by particle irradiation and thermal

TABLE III. Ground-state zero-field-splitting constants (D, E) of NV center configurations (Conf.) in 3C and 4H polytypes of SiC. The experimental data (D_e) in 3C were taken from Ref. [15]. The experimental data in 4H SiC recorded at cryogenic temperature are also provided as new results (D_e, E_e). In the ground state the two unpaired electrons are localized on the C atoms near Si vacancy, hence corresponding distances (d_1) are also given. For the off-axis configurations, two different C-C distances occur where the second distance is listed in the d_2 column. The larger the deviation is between d_1 and d_2 the larger is the E parameter.

Conf.	D (MHz)	E (MHz)	d_1 (Å)	d_2 (Å)	D_e (MHz)	E_e (MHz)
3C-kk	1409	0	3.34		1303	
4H-kk	1377	0	3.36		1282	0
4H-hh	1427	0	3.33		1331	0
4H-hk	1331	110	3.38	3.35	1193	104
4H-kh	1404	44	3.34	3.33	1328	15

TABLE IV. Calculated values of D and E parameters for NV center configurations (Conf.) in $6H$ SiC. Experimental values (D_e) are only available for the axial configurations [15]. Distances (d_1) of C-C atoms near Si vacancy are also listed. For the off-axis configurations, two different C-C distances occur where the second distance is listed in the d_2 column.

Conf.	D (MHz)	E (MHz)	d_1 (Å)	d_2 (Å)	D_e (MHz)
hh	1404	0	3.34		1328
k_1k_1	1348	0	3.36		1278
k_2k_2	1432	0	3.33		1345
k_1k_2	1404	145	3.35	3.33	
k_2h	1386	9	3.33	3.34	
hk_1	1352	14	3.34	3.35	

TABLE V. Calculated excited-state ^{3}E zero-field-splitting constants (D, E) of NV center configurations (Conf.) in $3C$ and $4H$ SiC. Distances between N and C atoms (N-C) around Si vacancy are also provided.

Polytype	Conf.	D (MHz)	E (MHz)	N-C (Å)
$3C$	kk	707.3	0	3.42
$4H$	kk	483.0	0	3.46
	hh	537.2	0	3.44
	hk	471.9	47.8	3.49
	kh	537.9	28.6	3.44

annealing. The observed EPR spectra are shown in Fig. 7. From these measurements, the D and E parameters for the basal NV configurations were extracted, and the low-temperature D parameters for all the four NV configurations in $4H$ SiC are shown in Table III. We note that the previously published EPR data for axial configurations in $4H$ SiC are those measured at $T = 300$ K in Ref. [15].

We showed above that proximate nuclear spins may reside around the electron spin of NV centers. The transfer of electron-spin polarization to neighboring nuclear spins is principally feasible for the NV center in $4H$ SiC and thus allows the realization of quantum memories. One possible method to spin polarize the proximate nuclear spins is the optical dynamic polarization via excited-state level anticrossing (ESLAC) [33,34]. We calculated the ZFS parameters of the ^{3}E excited states from which the required magnetic fields for ESLAC [35] can be obtained (see Table V). We emphasize that ZFS parameters in the excited state are subject to dynamic Jahn-Teller effect and can be temperature dependent, and our values are only valid at $T = 0$ K. In the excited state, the spin density is partially localized on the N atom, hence the distance between one of the C atoms and the N atom is given.

The intracenter optical transition of the NV centers is a key parameter for all quantum applications. The ZPL energies have been recently identified experimentally for the four different NV centers in $4H$ SiC [14]. We calculated the ZPL energies of NV centers in SiC that are associated with the energy difference between the ^{3}E excited state and $^3A_2$ ground state. The results are shown in Table VI, and once again we find a good agreement between calculated and experimental values. The discrepancy between the calculated and measured ZPL energies for each configuration is within 0.1 eV, that is expected from HSE06 hybrid density functional method [36]. However, the calculated differences between the ZPL energies of the defect configurations are technically converged within a few meV, in terms of the parameters of plane-wave supercell DFT method. We found that the 576-atom supercell with $2 \times 2 \times 2$ k-point sampling of Brillouin zone is at least required, in order to obtain the correct order of ZPL energies of the four defect configurations in $4H$ SiC.

Optically induced ground-state spin polarization has been observed by EPR for all NV centers in the three polytypes [13,15]. The ZPL energies correspond to the low-energy threshold of the optically induced ground-state spin polarization. This feature is a particularity of all NV centers in SiC and in diamond and allows the initialization of the ground-state spin configuration by an optical pulse. It is related to the existence of intermediate singlet states, which modify the recombination processes between the ^{3}E and $^3A_2$ states. The calculation of these highly correlated multideterminant singlet states is out of the scope of this paper.

V. DISCUSSION

In the following sections we discuss our results on the formation of NV centers in SiC (Sec. V A), the identification of individual NV centers in hexagonal SiC (Sec. V B), and

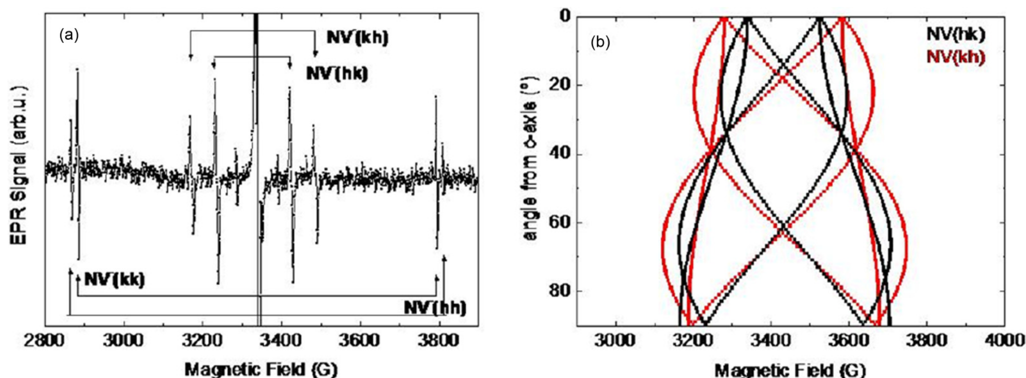

FIG. 7. (a) EPR spectrum of the NV center in $4H$ SiC displaying the two axial and two basal related EPR spectra for $\mathbf{B}\|c$ where $\mathbf{B}$ is the applied external magnetic field and c is the c axis of $4H$ SiC. (b) Simulated angular variation of the basal NV centers in $4H$ SiC.

TABLE VI. Zero-phonon-line (ZPL) energies of individual NV center configurations in 3*C* and 4*H* SiC. Calculated and experimental ZPL data (see Ref. [14]) are also presented.

Polytype	Conf.	ZPL (eV)	Signal	ZPL_{exp} (eV)
3*C*	*kk*	0.87		
4*H*	*hh*	0.966	PLX1	0.998
	kk	1.018	PLX2	0.999
	hk	1.039	PLX3	1.014
	kh	1.056	PLX4	1.051

the photoionization of NV centers in 4*H* SiC (Sec. V C). The results are compared to the properties of the closely related divacancy centers. Finally, we evaluate the stability of NV centers in the different SiC polytypes in Sec. V D.

A. Formation of NV centers in SiC

We consider the formation of NV centers in 4*H* SiC in two scenarios: (i) formation of NV centers as native defects related to growth conditions and (ii) NV centers formed by thermal diffusion of radiation induced Si vacancies in nitrogen doped material. We neglect the kinetic effects on the surface in this paper which might play a role in the first case.

Homo- and hetero-epitaxial high-quality thin films of SiC are generally grown by a chemical vapor deposition (CVD) process. If one approximates this CVD process as a thermal equilibrium process then the concentration of the in-grown defects can be estimated from their formation energies (see Fig. 8). We considered the formation of the NV center by nitrogen doping of 4*H* SiC. We assumed the incorporation of basic intrinsic defects, C vacancy, Si vacancy, the CAV complex, divacancy, as well as the substitutional nitrogen (N_C) and $(N_C)_4V_{Si}$ complexes beside the NV center, and finally N_CV_{Si} complexes. The simulations were carried out at different growth temperatures between 1600 and 2000 °C, typical of CVD growth of SiC. The results are plotted in Fig. 9.

It follows that the concentration of in-grown Si vacancies, CAV complexes, and divacancies is negligible. $(N_C)_4V_{Si}$ complexes have the lowest formation energy of ~1 eV and exhibit the highest concentration (over 10^{19} cm^{-3}), which explains the known doping limitation of nitrogen in SiC (see Ref. [29]). The $(N_C)_4V_{Si}$ defect is electrically inactive with exhibiting $S = 0$ spin state, thus it does not establish an undesirable electron-spin bath for qubit application of N_CV_{Si}. The maximum concentration of neutral N_C is around 10^{18} cm^{-3}. The neutral N_C has an $S = 1/2$ spin. The C vacancy has a higher concentration than that of NV complexes. Nevertheless, C vacancies will be double negatively charged at these doping conditions with a diamagnetic ground state. It is important to note that the concentration of the NV complex is about seven to nine orders of magnitude smaller than that of the N_C. In this condition, the majority of the NV complex will be in the double negative charge state with $S = 1/2$ spin and not in the desired single negative charge state. Whereas such low defect concentrations can be detected by PL spectroscopy, they are well below the detection limit of EPR spectroscopy. At lower temperature growth (<1600 °C) the total concentration of the NV center will further decrease and be in the region where NV centers will occur as single NV centers. They can be detected by confocal PL microscopy but they have not yet been reported. However, the large concentration of neutral N_C introduces a dense electron-spin bath that is detrimental for single NV center ODMR measurements, because this can significantly reduce the electron-spin coherence time.

The second approach, the one which has been successfully used in the past, is to start with lightly (10^{16} cm^{-3}) nitrogen doped SiC samples; then by ion implantation or particle irradiation Si vacancies can be created; NV center formation is obtained by thermal annealing in a temperature range where Si vacancies become mobile. The first experimental results of NV centers in 4*H* SiC were obtained on proton irradiated N-doped samples [13,15]. We note that irradiation or implantation creates vacancies and interstitials in both sublattices. Regarding the monovacancies, it is expected that due to the lower displacement energies of C atoms compared with Si atoms [37–40] more C vacancies than Si vacancies are created by irradiation or implantation. Thus, divacancies can also be formed when Si vacancies become mobile during annealing at around 750 °C [41,42]. In order to study the formation of NV centers, we calculated the binding energies of the N_C and Si vacancy versus that of the C vacancy and Si vacancy [see Figs. 8(a)–8(c) and the derived plots in Fig. 10]. Our results show that the binding energy for divacancies is always higher than for NV centers; consequently the formation of divacancies has a higher probability provided that C vacancies are available for the mobile Si vacancies. If the initial concentration of nitrogen is higher than that of C vacancies then the relative concentration of divacancies and NV complexes may be tuned toward the preferential formation of NV centers. This scenario is the one used for the formation of large ensembles of NV centers. Indeed, the previous EPR and PL investigations always showed the presence of divacancies beside NV centers [13,15]. Since divacancies have a nonzero spin in their various charge states and are optically active, they can influence the electron-spin coherence time and the photostability of the NV center. The latter will be discussed below. Clearly for the formation of individual NV centers different nanoscopic approaches have to be applied, like low dose implantation of N_2 ions into nondoped SiC.

B. Spectroscopy of individual NV centers in hexagonal SiC

The magneto-optical parameters of a large ensemble of NV centers in 4*H* SiC are known from EPR and PL studies [13–15], however future quantum technology applications will be based on the spectroscopy of individual NV centers. Therefore, it is of high importance to identify the individual NV centers in 4*H* SiC.

We study first the magnetic properties. As with the spin density associated with hyperfine couplings, so the spin-density matrix associated with ZFS is mostly localized on the carbon dangling bonds of the Si vacancy in the ground state of the NV center (see Fig. 6). The experimentally determined [13,15] *g*-tensor anisotropy implies that the second-order spin-orbit coupling may be not negligible, that may contribute to the ZFS. Furthermore, the first order spin-orbit coupling might contribute to the ZFS in the off-axis configurations

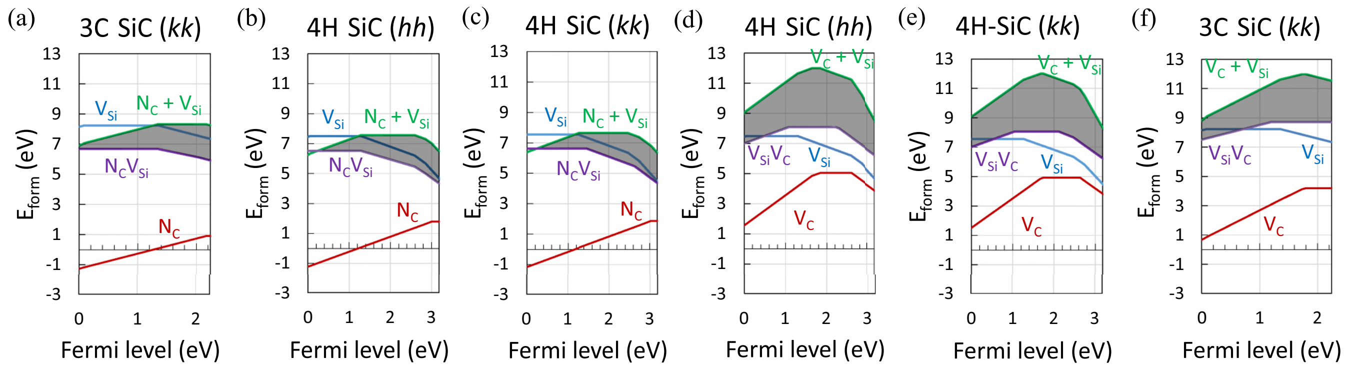

FIG. 8. Formation energies of axial (a)–(c) NV centers and (d)–(f) divacancies as a function of the Fermi level in 3*C* and 4*H* polytypes. Shaded areas represent the stability of the corresponding complexes.

with C_{1h} symmetry. Nevertheless, the vast majority of ZFS involves the electron-spin–electron-spin–dipolar interaction, that we can fairly well calculate within Kohn-Sham DFT.

First, we discuss the on-axis configurations. The distance between carbon dangling bonds is shorter at the *hh* site than that at the *kk* site (see Table III), and correspondingly the *D* constant is larger at the *hh* site than that at the *kk* site. Indeed, we find the calculated *D* constant in *hh* configuration to be the highest one. This is very similar to the case of the divacancy in 4*H* SiC [43]. Regarding the off-axis configurations, the *E* constant is a good parameter to distinguish the N_CV_{Si} *kh* and *hk* configurations. The *kh* configuration has always a smaller *E* constant than the *hk* configuration (see Table III). The *hh* and *kk* sites can be also distinguished by their strong ^{13}C and ^{29}Si hyperfine interactions. Basically, the spin density is more localized in the *hh* configuration than in *kk* configurations. Accordingly, the corresponding ^{13}C hyperfine constants are higher whereas the ^{29}Si hyperfine constants are smaller in *hh* configuration than those in *kk* configuration. In summary, the ground-state parameters of NV centers in 4*H* SiC allow a simple distinction between the four configurations. The ≈100-MHz systematic discrepancy between the calculated and experimentally determined *D* constants might be partially attributed to the neglect of second-order spin-orbit interaction.

Another important fingerprint of the NV centers is their photoluminescence spectrum. At low temperatures, the ZPL energies in the PL spectrum of NV centers have been identified in 4*H* SiC [14]. The calculated absolute values of the ZPL energies are close to the experimental ones (see Table VI). However, the calculated site dependence of the ZPL energies is not so well reproduced by the calculations. The ZPL energy difference between the PLX1 and PLX2 NV centers is only 1 meV. It is extremely challenging to reach such an accuracy in the calculation. We find that the *hh* and *kk* NV center configurations have the lowest ZPL energies, as was previously suggested [13,15]. Thus, PLX1 and PLX2 should be associated with the axial configurations. Our calculations imply that the *hh* configuration has the lowest ZPL energy, nevertheless the identification of PLX1 does not stand on solid ground based on solely the calculated ZPL. In analogy with the divacancy, for which ODMR measurements under resonant excitation have been performed, the *hh* configuration should have the lowest ZPL energy and the largest *D* constant [43]. By assuming the same trends for the NV center, we deduce that the *hh* configuration should be associated with the PLX1 spectrum and *kk* should be associated with the PLX2 spectrum. The PLX3 and PLX4 ZPLs should be associated with the off-axis NV center configurations. Our calculations imply that N_CV_{Si} *hk* and *kh* configurations can be associated with PLX3 and PLX4 PL centers, respectively.

We also show the calculated ZFS parameters for the ground state of NV centers in 6*H* SiC (see Table IV). Interestingly, the

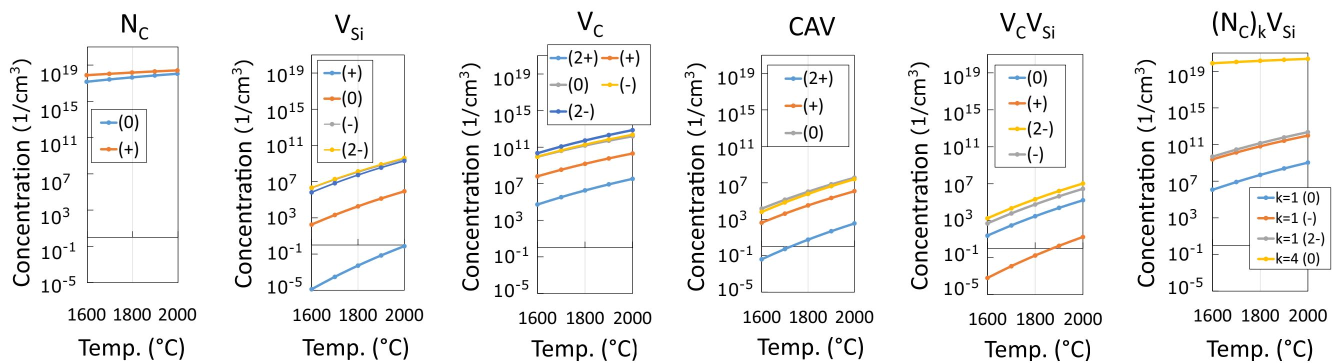

FIG. 9. Concentration of technologically important defects in 4*H* SiC as a function of growth temperature. All the relevant charge states and configurations of each defect are considered. The concentration was calculated in thermal equilibrium assuming stoichiometric SiC. Please note the logarithmic scale on the concentration.

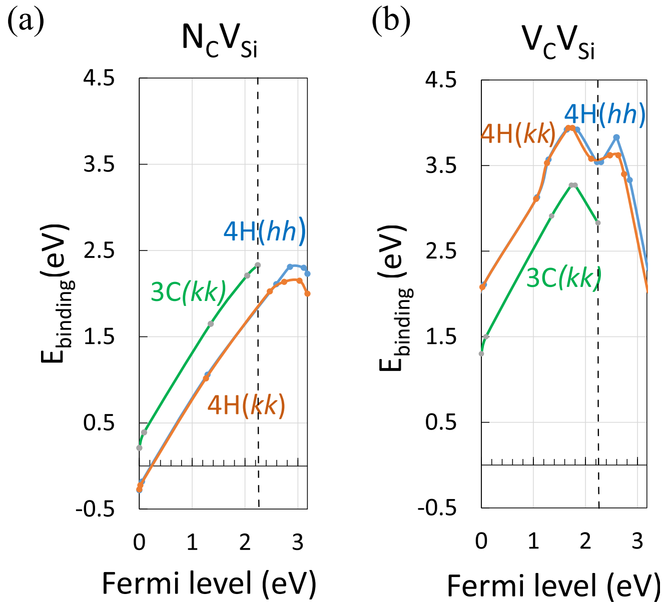

FIG. 10. Binding energies as a function of Fermi level for axial (a) NV center and (b) divacancy configurations in $3C$ and $4H$ SiC. Dashed lines represent the conduction-band minimum of the $3C$ polytype that lies lower than that of $4H$ SiC.

k_2k_2 configuration has the largest D constant which is followed by that of hh and k_1k_1 configurations in descending order. This can be directly compared to the experimental assignments [15]. In the $6H$ polytype the k_1k_2 off-axial configuration has the largest E value which is followed by that of hk_1 and k_2h configurations in descending order. The PL spectrum of the NV centers in $6H$ SiC has not yet been reported.

C. Photoionization of NV centers in 4H SiC

The photostability and spectral stability of solid-state qubits is of high importance. The photostability of NV centers might be compromised by simultaneous photoionization. The photoionization energies are given in Table I: the NV center in a negative charge state NV(−) can be photoionized to neutral charge state NV(0) by promoting an electron to the conduction-band edge with an energy of about 1.7–1.8 eV. This energy is sufficient to reionize NV(0) to NV(−) by promoting an electron from the valence band to the in-gap defect level. In the case of single defect spectroscopy, confocal microscopy is applied with high excitation power that can result in two-photon absorption processes. According to our results, the two-photon absorption process will also give rise to photoionization. Unfortunately, the excitation energy of NV(0) is not known and cannot be calculated by Kohn-Sham DFT. Therefore, the threshold energy to reionize NV(0) to NV(−) by two-photon absorption is not known. If the ZPL energy of NV(0) is higher than that of NV(−) then NV(−) should be excited into the phonon sideband, in order to reionize NV(0) to NV(−) by two-photon absorption.

Spectral diffusion in the emission of the single NV(−) center might occur upon photoexcitation when nearby defects are simultaneously excited, resulting in fluctuating charges in the proximity of the NV(−) center. These fluctuating charges can shift the ZPL energy of NV(−) by small amounts, which is detrimental for quantum applications. We showed above that the divacancy defect will form together with NV centers under implantation or irradiation induced formation. Our calculations show that if divacancies are excited by about 1.1 eV two-photon absorption can also occur, which leads to the ionization of the neutral divacancy [see Fig. 5(c)]. The same photon energy is sufficient to excite NV(−) in the phonon sideband. Our calculations imply that excitation energy lower than 1.1 eV should be applied, in order to avoid the photoionization of the divacancies.

We may conclude by emphasizing the two conditions for the optimal readout process of NV qubits in $4H$ SiC: (i) efficient reionization of NV(−) and (ii) conserving spectral stability by avoiding ionization of the divacancy by two-photon absorption.

D. Comparison of SiC polytypes to host NV qubits

We previously discussed the photostability and spectral stability of NV qubits in $4H$ SiC in detail. Here, we further discuss this issue for NV qubits in $3C$ and $6H$ SiC.

In $3C$ SiC, the calculated acceptor level of the NV defect lies at about 1.5 eV with respect to the valence-band edge, similarly to the NV defects in the hexagonal polytypes. Since the band gap of $3C$ SiC is smaller, 2.4 eV at low temperatures, the ZPL energy for the intracenter transition and the ionization energy of NV(−) almost coincide. Thus excitation of the NV center in $3C$ SiC results in an excited state resonant with the conduction-band edge. In this case the photostability of NV(−) in $3C$ SiC may be difficult to maintain, particularly, at elevated temperatures. We note that the ensembles of NV centers could be efficiently optically spin polarized in N-doped $3C$ SiC [15]. Nevertheless, this process might involve recapture of free electrons created by photoexcitation, that may not efficiently work at the single defect level. On the other hand, if a spin-selective photoionization occurs for this defect then photoionization based detection of magnetic resonance could be the appropriate methodology [44] to read out the spin of the single NV qubit.

The band gap of $6H$ SiC is about 0.25 eV lower than that of $4H$ SiC. The acceptor levels with respect to the valence-band edges and excitation energies of the NV defects are very similar in the two polytypes. As a consequence, the two-photon absorption of the NV(−) defect in $6H$ SiC may be more effective than that in $4H$ SiC because of the larger density states in the conduction bands of $6H$ SiC. Thus, the relative rates of ionization and reionization of NV(−) centers in $6H$ SiC may shift toward the ionization and compromise the stability of NV centers in $6H$ SiC. If NV(−) is excited with an energy above the ZPL energy of divacancy then two-photon ionization of neutral divacancy can take place because of the relatively low-lying conduction-band edge of $6H$ SiC. We conclude that our calculations imply that $4H$ SiC with the largest band gap is the optimal host for NV center qubit applications with optical readout.

VI. SUMMARY

In summary, we carried out DFT calculations of N_CV_{Si} defects in $3C$, $4H$, and $6H$ SiC. We focused on the negatively charged N_CV_{Si} defect, i.e., the NV center with potential qubit applications. We discussed the formation of the NV center in SiC, and found the divacancy inevitably forms when the NV center is produced by implantation or irradiation. We calculated the ground-state and excited-state magneto-optical properties of the NV centers and compared them with the experimental magneto-optical data. We identified the individual NV qubits in hexagonal polytypes. We also discussed the photoionization and spectral stability of the NV center in SiC. Our results show the importance of selective photoexcitation avoiding simultaneous excitation of divacancies in the two-photon absorption process.

ACKNOWLEDGMENTS

A.C. acknowledges the Ministry of Human Resources for financial support in the framework of the National Talent Program (Grant No. NTP-NFTÖ-16-0118). A.G. acknowledges Hungarian NKFIH Grant No. NVKP_16-1-2016-0152958.

[1] J. R. Weber, W. F. Koehl, J. B. Varley, A. Janotti, B. B. Buckley, C. G. Van de Walle, and D. D. Awschalom, Proc. Natl. Acad. Sci. USA **107**, 8513 (2010).

[2] D. DiVincenzo, Nat. Mater. **9**, 468 (2010).

[3] H. J. Mamin, M. Kim, M. H. Sherwood, C. T. Rettner, K. Ohno, D. D. Awschalom, and D. Rugar, Science **339**, 557 (2013).

[4] M. W. Doherty, N. B. Manson, P. Delaney, F. Jelezko, J. Wrachtrup, and L. Hollenberg, Phys. Rep. **528**, 1 (2013).

[5] T. D. Ladd, F. Jelezko, R. Laflamme, Y. Nakamura, C. Monroe, and J. L. O'Brien, Nature (London) **464**, 45 (2010).

[6] S. Hong, M. S. Grinolds, L. M. Pham, D. Le Sage, L. Luan, R. L. Walsworth, and A. Yacoby, MRS Bull. **38**, 155 (2013).

[7] W. F. Koehl, B. B. Buckley, F. J. Heremans, G. Calusine, and D. D. Awschalom, Nature (London) **479**, 84 (2011).

[8] A. Gali, Phys. Status Solidi B **248**, 1337 (2011).

[9] A. L. Falk, B. B. Buckley, G. Calusine, W. F. Koehl, V. V. Dobrovitski, A. Politi, C. A. Zorman, P. X.-L. Feng, and D. D. Awschalom, Nat. Commun. **4**, 1819 (2013).

[10] D. J. Christle, P. V. Klimov, C. F. de las Casas, K. Szász, V. Ivády, V. Jokubavicius, J. Ul Hassan, M. Syväjärvi, W. F. Koehl, T. Ohshima, N. T. Son, E. Janzén, Á. Gali, and D. D. Awschalom, Phys. Rev. X **7**, 021046 (2017).

[11] B. Somogyi, V. Zolyomi, and A. Gali, Nanoscale **4**, 7720 (2012).

[12] B. Somogyi and A. Gali, J. Phys.: Condens. Matter **26**, 143202 (2014).

[13] H. J. von Bardeleben, J. L. Cantin, E. Rauls, and U. Gerstmann, Phys. Rev. B **92**, 064104 (2015).

[14] S. A. Zargaleh, B. Eble, S. Hameau, J.-L. Cantin, L. Legrand, M. Bernard, F. Margaillan, J.-S. Lauret, J.-F. Roch, H. J. von Bardeleben, E. Rauls, U. Gerstmann, and F. Treussart, Phys. Rev. B **94**, 060102 (2016).

[15] H. J. von Bardeleben, J. L. Cantin, A. Csóré, A. Gali, E. Rauls, and U. Gerstmann, Phys. Rev. B **94**, 121202 (2016).

[16] X. Wang, M. Zhao, H. Bu, H. Zhang, X. He, and A. Wang, J. Appl. Phys. **114**, 194305 (2013).

[17] L. Gordon, A. Janotti, and C. G. Van de Walle, Phys. Rev. B **92**, 045208 (2015).

[18] J. Heyd, G. E. Scuseria, and M. Ernzerhof, J. Chem. Phys. **118**, 8207 (2003).

[19] J. P. Perdew, K. Burke, and M. Ernzerhof, Phys. Rev. Lett. **77**, 3865 (1996).

[20] V. Ivády, T. Simon, J. R. Maze, I. A. Abrikosov, and A. Gali, Phys. Rev. B **90**, 235205 (2014).

[21] P. E. Blöchl, Phys. Rev. B **50**, 17953 (1994).

[22] G. Kresse and J. Furthmüller, Phys. Rev. B **54**, 11169 (1996).

[23] C. Freysoldt, J. Neugebauer, and C. G. Van de Walle, Phys. Rev. Lett. **102**, 016402 (2009).

[24] K. Szász, T. Hornos, M. Marsman, and A. Gali, Phys. Rev. B **88**, 075202 (2013).

[25] S. B. Zhang and J. E. Northrup, Phys. Rev. Lett. **67**, 2339 (1991).

[26] B. Aradi, A. Gali, P. Deák, J. E. Lowther, N. T. Son, E. Janzén, and W. J. Choyke, Phys. Rev. B **63**, 245202 (2001).

[27] A. J. Steckl, J. Devrajan, S. Tlali, H. E. Jackson, C. Tran, S. N. Gorin, and L. M. Ivanova, Appl. Phys. Lett. **69**, 3824 (1996).

[28] O. Kordina, C. Hallin, A. Henry, J. P. Bergman, I. Ivanov, A. Ellison, N. T. Son, and E. Janzén, Phys. Status Solidi B **202**, 321 (1997).

[29] M. Bockstedte, A. Mattausch, and O. Pankratov, Appl. Phys. Lett. **85**, 58 (2004).

[30] E. Rauls, T. Lingner, Z. Hajnal, S. Greulich-Weber, T. Frauenheim, and J.-M. Spaeth, Phys. Status Solidi B **217**, r1 (2000).

[31] S. Castelletto, B. C. Johnson, V. Ivády, N. Stavrias, T. Umeda, A. Gali, and T. Oshima, Nat. Mater. **13**, 151 (2013).

[32] K. Szász, V. Ivády, I. A. Abrikosov, E. Janzén, M. Bockstedte, and A. Gali, Phys. Rev. B **91**, 121201 (2015).

[33] V. Jacques, P. Neumann, J. Beck, M. Markham, D. Twitchen, J. Meijer, F. Kaiser, G. Balasubramanian, F. Jelezko, and J. Wrachtrup, Phys. Rev. Lett. **102**, 057403 (2009).

[34] A. L. Falk, P. V. Klimov, V. Ivády, K. Szász, D. J. Christle, W. F. Koehl, A. Gali, and D. D. Awschalom, Phys. Rev. Lett. **114**, 247603 (2015).

[35] V. Ivády, K. Szász, A. L. Falk, P. V. Klimov, D. J. Christle, E. Janzén, I. A. Abrikosov, D. D. Awschalom, and A. Gali, Phys. Rev. B **92**, 115206 (2015).

[36] P. Deák, B. Aradi, T. Frauenheim, E. Janzén, and A. Gali, Phys. Rev. B **81**, 153203 (2010).

[37] W. J. Choyke, in *Radiation Effects in Semiconductors, 1976*, edited by N. B. Urli and J. W. Corbet, Inst. Phys. Conf. Ser. No. 31 (Institute of Physics, London, 1977), p. 58.

[38] J. W. Steeds, F. Carosella, G. A. Evans, M. M. Ismail, L. R. Danks, and W. Voegeli, Mat. Sci. Forum **353**, 381 (2001).

[39] G. A. Evans, J. W. Steeds, L. Ley, M. Hundhausen, N. Schulze, and G. Pensl, Phys. Rev. B **66**, 035204 (2002).

[40] G. Lucas and L. Pizzagalli, Phys. Rev. B **72**, 161202 (2005).

[41] E. Sörman, N. T. Son, W. M. Chen, O. Kordina, C. Hallin, and E. Janzén, Phys. Rev. B **61**, 2613 (2000).

[42] M. Bockstedte, A. Mattausch, and O. Pankratov, Phys. Rev. B **68**, 205201 (2003).

[43] A. L. Falk, P. V. Klimov, B. B. Buckley, V. Ivády, I. A. Abrikosov, G. Calusine, W. F. Koehl, A. Gali, and D. D. Awschalom, Phys. Rev. Lett. **112**, 187601 (2014).

[44] E. Bourgeois, A. Jarmola, P. Siyushev, M. Gulka, J. Hruby, F. Jelezko, D. Budker, and M. Nesladek, Nat. Commun. **6**, 8577 (2015).